reactions

MDPI

Article

Confinement of $LiAlH_4$ in a Mesoporous Carbon Black for Improved Near-Ambient Release of H_2

Pavle Ramah [1], Rasmus Palm [1,2,*], Kenneth Tuul [1], Jaan Aruväli [3], Martin Månsson [2] and Enn Lust [1]

[1] Institute of Chemistry, University of Tartu, Ravila 14a, 50411 Tartu, Estonia
[2] Department of Applied Physics, KTH Royal Institute of Technology, SE-106 91 Stockholm, Sweden
[3] Institute of Ecology and Earth Sciences, University of Tartu, Ravila 14a, 50411 Tartu, Estonia
* Correspondence: rasmus3@kth.se

Abstract: $LiAlH_4$ is a potential solid-state H_2 storage material, where safe and efficient H_2 storage is of critical importance for the transition towards a sustainable emission-free economy. To improve the H_2 release and storage properties of $LiAlH_4$, confinement in porous media decreases the temperature of H_2 release and improves the kinetics, where considerably improved H_2 release properties are accompanied by a loss in the total amount of H_2 released. The capability of mesoporous carbon black to improve the H_2 storage properties of confined $LiAlH_4$ is investigated with temperature-programmed desorption and time-stability measurements using X-ray diffraction and N_2 gas adsorption measurements to characterize the composite materials' composition and structure. Here, we present the capability of commercial carbon black to effectively lower the onset temperature of H_2 release to that of near-ambient, $\geq$295 K. In addition, the confinement in mesoporous carbon black destabilized $LiAlH_4$ to a degree that during $\leq$14 days in storage, under Ar atmosphere and at ambient temperature, 40% of the theoretically contained H_2 was lost due to decomposition. Thus, we present the possibility of destabilizing $LiAlH_4$ to a very high degree and, thus, avoiding the melting step before H_2 release at around 440 K using scaffold materials with fine-tuned porosities.

Keywords: H_2 storage; complex metal hydride; $LiAlH_4$; nanoconfinement; temperature-programmed desorption; X-ray diffraction; N_2 adsorption; time-stability

check for updates

Citation: Ramah, P.; Palm, R.; Tuul, K.; Aruväli, J.; Månsson, M.; Lust, E. Confinement of $LiAlH_4$ in a Mesoporous Carbon Black for Improved Near-Ambient Release of H_2. *Reactions* **2023**, *4*, 635–646. https://doi.org/10.3390/reactions4040035

Academic Editors: Valérie Meille, Francesco Frusteri and Sibudjing Kawi

Received: 11 August 2023
Revised: 5 September 2023
Accepted: 7 October 2023
Published: 11 October 2023

1. Introduction

H_2 is a vital component for the transition towards a net zero CO_2 emission economy [1–3]. A crucial part of the transition towards an H_2-based economy is the use of safe, efficient, and energy-dense long- and short-term H_2 storage solutions [2–4]. Contemporary commercialized methods for H_2 storage, i.e., H_2 gas pressurization and H_2 liquefaction, embody multiple critical problems hindering their widespread use, which is necessary for the transition towards an H_2-based economy. For example, the extreme pressure and/or temperature conditions required for storage, high energy use for pressurization and liquefaction of H_2, high cost of containers capable of tolerating pressurized or liquefied H_2, and safety hazards associated with H_2 leakage, H_2 embrittlement, and extreme storage pressure and temperature conditions are limiting factors towards the rapid expansion and utilization of a H_2-based economy [3–5].

Solid-state H_2 carriers are highly promising alternative solutions that show promise for the potentially low pressure of H_2 required for storage, high volumetric and gravimetric H_2 density, and enhanced safety through controlled release of H_2 from the solid state [3,4]. Complex metal hydride $LiAlH_4$ is one such promising candidate for H_2 storage, as it exhibits a high gravimetric and volumetric H_2 density, 10.54 mass% and 96.6 g L^{-1}, respectively; is composed of abundant elements; and has low enthalpies of decomposition, 9.8 and 15.7 kJ mol^{-1}, for the first two H_2 release steps (R1 and R2), respectively [6].

$$3LiAlH_4 \rightarrow Li_3AlH_6 + 2Al + 3H_2 \qquad 5.27\ \text{mass\% of } H_2 \text{ released by end} \qquad \text{(R1)}$$

$$Li_3AlH_6 \rightarrow 3LiH + Al + 1\frac{1}{2}H_2 \quad \text{7.91 mass\% of } H_2 \text{ released by end} \tag{R2}$$

$$3LiH \rightarrow 3Li + 1\frac{1}{2}H_2 \quad \text{10.54 mass\% of } H_2 \text{ released by end} \tag{R3}$$

The main obstruction to the applicability of $LiAlH_4$ as a solid-state H_2 storage material is the relatively high temperature of H_2 release [7–11], e.g., the majority of H_2 is released around 437 K, at a heating rate of 2 K min^{-1}, and corresponding to R1 (Figure 1). The temperature for the release of H_2 from the first decomposition reaction, R1, matches that of melting of $LiAlH_4$, where melting of $LiAlH_4$ is brought forth before R1 in the case of heating rates $\geq$ 2.5 K min^{-1} [8]. The preliminary melting at higher heating rates causes the R1 reaction to become exothermic, as it is preceded by endothermic melting [8,11]. Regardless of the kinetic limitation, where clear decomposition of $LiAlH_4$ starts after melting and bulk $LiAlH_4$ is stable at ambient temperature, bulk $LiAlH_4$ has been shown to desorb 7.1 mass% of H_2 at 393 K within 72 h when stored under 0.1 MPa of H_2 [11].

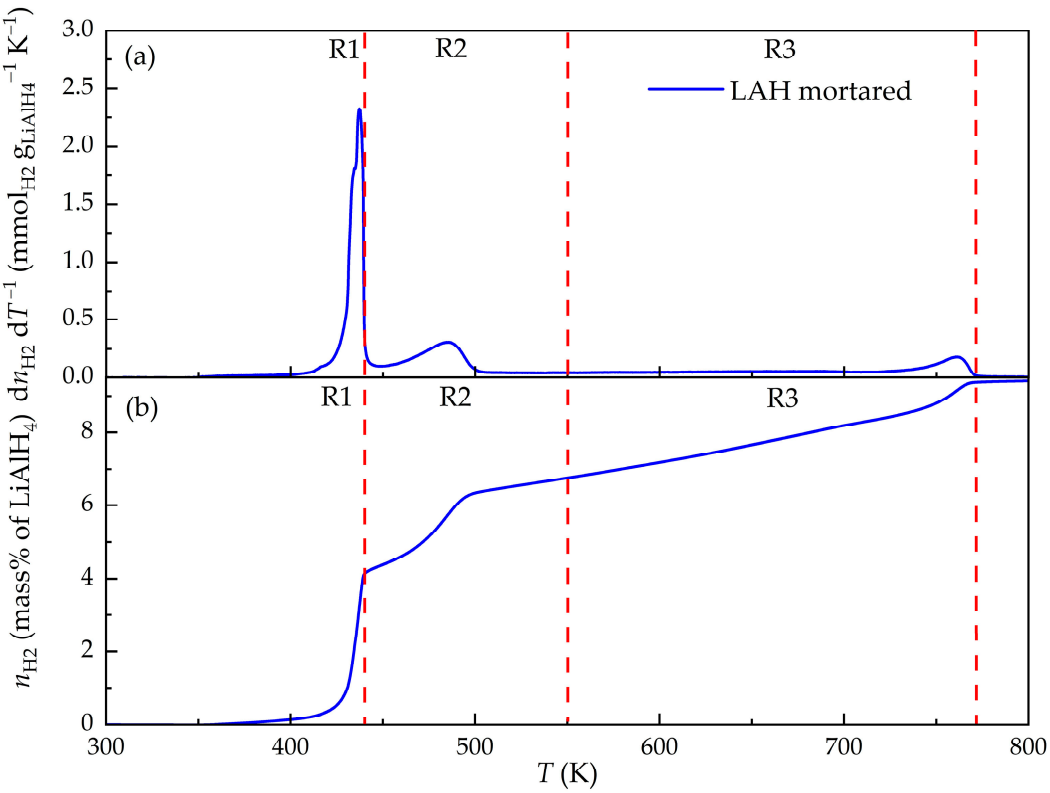

Figure 1. Temperature-programmed desorption of mortared $LiAlH_4$ (LAH mortared) measured at a temperature ramp rate of 2 K min^{-1} and presented as differential (**a**) and cumulative (**b**) amounts of H_2 released. The red dashed lines correspond to the idealized temperature regions of the three decomposition reaction steps (R1–R3). The lower yield of H_2 in comparison to the theoretical maximum, 10.54 mass% of H_2 from $LiAlH_4$, was assigned to the pre-measurement occurrence of the first decomposition step (R1), and thus, the R1 temperature region was decreased accordingly.

The release of H_2 after melting from bulk $LiAlH_4$ at higher temperature scan rates, $\geq$1 K min^{-1}, was shown to be kinetically more favourable, as the activation energy decreased from 162 to 115 kJ mol^{-1} when hydrogen release was brought forth after melting through the use of higher temperature scan rates [8,11]. The activation energies of the decomposition steps R2 and R3 in bulk $LiAlH_4$ are practically equivalent, at 86 kJ mol^{-1} [8]. Thus, to improve the kinetics and to bring forth the low-temperature release of H_2 from

$LiAlH_4$, various methods have been used to eliminate the phase-transition-induced kinetic limitation.

Confinement inside a porous scaffold, addition of catalysts, and mixing with other complex metal hydrides have been used for this effect to decrease the temperature of H_2 release, improve the kinetics, and improve cyclability through hydrogenation at lower H_2 pressure and temperature conditions by weakening the Al-H bond [10,12–21]. For example, the addition of nano-sized TiH_2 [17] and nano-sized TiC [18] decreased the onset temperature of H_2 release down to 350 K, and the majority of H_2 from decomposition steps R1 and R2 was released during 15 min at 393 K. A part in the catalytic effect was attributed to the weakening of the Al-H bonds, where the Al-H band in infrared spectroscopy shifted to higher frequencies when TiC doping was applied [18]. Alternatively, an abrupt release over several seconds of 5.7 mass% of H_2 at 335 K was achieved with the addition of fluorographites [19]. This is achieved as the fluorographite reacts with $LiAlH_4$, forming LiF and Al_4C_3 in a highly exothermic reaction, −178 kJ mol^{-1}, and as such is irreversible and hard to control in a H_2 storage system [19]. The addition of a TiF_3 catalyst has been shown to destabilize $LiAlD_4$ to a degree where, over a storage period of 6 months, the $LiAlD_4$ + TiF_3 sample completely decomposed to LiD and Al [21].

Confinement of $LiAlH_4$ in various porous carbonaceous materials has been shown to decrease the temperature of H_2 release and to improve the kinetics of H_2 release by weakening the Al-H bonds, nano-sizing effects, improved solid-gas interactions, and shorter diffusion paths for ions [13–15]. With the use of only 10 mass% of activated carbon addition, the onset temperature of H_2 release decreased to 373 K for R1 and 430 K for R2 and was accompanied by a decrease in the activation energy from 91 kJ mol^{-1} to 70 kJ mol^{-1} and from 100 kJ mol^{-1} to 85 kJ mol^{-1} for the first two decomposition reactions, R1 and R2, respectively [13]. Mesoporous carbon with N defect sites as a scaffold for $LiAlH_4$ confinement has been shown to be reversibly hydrogenated under 100 MPa of H_2 with a yield of 80%, where the reversible hydrogenation of $LiAlH_4$ after the release of H_2 has been a major hurdle for the use of $LiAlH_4$ as a H_2 storage material [12]. This was brought forth by the strong Li–N interactions of Li in $LiAlH_4$ and N sites in the carbon material, respectively, where the Li adatoms remained bound at the pyridinic N defects over performed (de)hydrogenation cycles and caused the bypassing of decomposition step R1, where no intermediate Li_3AlH_6 was formed [12]. The bypassing of the first decomposition step, R1, has also been reported in the case of nanoconfined $NaAlH_4$ [22]. Partial hydrogenation of H_2 of dehydrogenated $LiAlH_4$ at 423 K and 8 MPa has been reported when 22 mass% of $LiAlH_4$ solution was impregnated into hollow carbon nanospheres, whereas this was achieved only for a low fraction of theoretical H_2 present in pristine composite and 0.4 mass% of H_2 of the total mass of composite [14]. In a more persuasive case, $LiAlH_4$ confined in a high surface area graphite was shown to exhibit a reversible hydrogen capacity of 0.6 mass% at 573 K and under 7 MPa of H_2 pressure and mainly contributed to the reversible decomposition step R2 [15].

In the case of a similar complex metal hydride, $NaAlH_4$, it has been shown that confinement inside a microporous carbon material lowers the onset of hydrogen release down to almost ambient temperature, supports the formation of distinct $NaAlH_4$ phases with different H_2 release kinetics, and causes the disappearance of crystalline/small-particulate $NaAlH_4$ and decomposition product phases over multiple cycles [23,24]. In the case of confinement of $NaAlH_4$ in a mesoporous carbon black, the hydrogenation at relatively mild pressure, 6 MPa, and temperature, 423 K, conditions were achieved with the separation of Na_3AlH_6, a product of the second decomposition step (R2), where the quick and reversibility of the R2 step was shown with in situ neutron diffraction [25,26].

Thus, the effect of $LiAlH_4$ confinement in a mesoporous carbon black is investigated with the same commercial mesoporous carbon black, Vulcan XC72, used with $NaAlH_4$ [25,26]. The goal is to yield similar or superior effects for the improvement of H_2 release properties to those achieved in the case of $NaAlH_4$. It has been shown previously that in the case of nanoconfinement of complex metal hydrides, $LiAlH_4$ and

$NaAlH_4$, the onset temperature of H_2 release is near-ambient, and a considerable amount of theoretically contained H_2 is lost by the time of H_2 release measurements, especially at lower hydride mass% loadings [23,25]. Thus, to determine if the efficiency loss is caused by the destabilization of $LiAlH_4$, similar to that currently achieved by a TiF_3 catalyst [21], the loss of H_2 storage efficiency during ball-milling synthesis and storage is determined for different $LiAlH_4$ mass% composites. Insight is presented into the root cause of H_2 storage efficiency loss in the case of confinement in mesoporous carbon materials, and problematic points for testing such materials are discussed.

2. Materials and Methods

2.1. Synthesis

All precursor chemical and sample storage, preparation, and retrieval was performed under an argon atmosphere (Ar, 5.0, Linde, Basingstoke, UK) in a MBraun LABmaster sp glovebox (MBraun, Garching bei München, Germany). Lithium alanate ($LiAlH_4$, Sigma Aldrich, St. Louis, MO, USA, pellets, reagent grade, 95%) was mortared (LAH mortared) by hand to crush the pellets into smaller particles usable for further characterization and synthesis routines. The mesoporous carbon black (MCB) Vulcan XC72R (Cabot, AR, USA) was degassed at 120 °C and under 100 mbar vacuum for 24 h before transfer to the glovebox. Vulcan XC72R has been shown to have low amounts of impurities and minimal amounts of functional groups [27,28]. The composites were prepared by combining the LAH mortared with Vulcan XC72R MCB in a Pulverisette 6 classic line (Fritsch, Idar-Oberstein, Germany) planetary mono mill for a total milling time of 40 min. The 40 min milling time was made up of 8 milling cycles, 5 min each, and at 400 rpm, with 10 min of rest for cooling between each milling cycle. A ZrO_2 grinding bowl with 25 ZrO_2 10 mm diameter grinding balls was used. The ball mill grinding vessel was hermetically sealed with a mechanical clamp under an Ar atmosphere inside a glovebox. LAH mortared/MCB composites containing 20 to 80 mass% of $LiAlH_4$ in the final composite were prepared following the aforementioned ball-milling routine, where the final composites are noted as LAH x, where x is the mass% of $LiAlH_4$ in the final composite based on the initial weighting of the added $LiAlH_4$.

2.2. N_2 Adsorption

N_2 gas adsorption measurements at 77 K were performed with a 3FLEX (Micromeritics, Norcross, GA, USA) adsorption analyzer. The sample holder was filled with approximately 150 mg of the sample inside a glovebox under an Ar atmosphere. The sample holder was hermetically sealed and transferred to the instrument and degassed at 313 K under a vacuum of at least 1 Pa for 24 h before the measurement. The specific surface area (S_{BET}) was calculated according to the BET theory [29], and the pore volumes (V_{pore}) were calculated from the amount of adsorbed N_2 at relative pressure, p/p°, of 0.95 [29]. The V_{pore} value obtained at p/p° = 0.95 corresponds to the volume of pores with widths up to ~40 nm.

2.3. X-ray Diffraction

The X-ray diffraction (XRD) measurements were performed with a D8 Advance (Bruker, Mannheim, Germany) diffractometer using a low-background airtight specimen holder. The samples were prepared inside a glovebox under an Ar atmosphere. The D8 Advanced diffractometer was equiped with Ni-filtered Cu Kα radiation in combination with a LynxEye detector. XRD measurements were performed in the 2θ range from 13 to 80°, with a step size of 0.016°. XRD data analysis was performed with the software package Diffrac Suite EVA (Version 6.0.0.6, 2021 Relase) and the PDF4+ 2020 database [30].

2.4. Temperature-Programmed Desorption

Temperature-programmed desorption (TPD) measurements were performed with an AutoChem 2950 HP (Micromeritics, Norcross, GA, USA) chemisorption analyzer, which uses a thermal conductivity detector to quantitatively determine changes in the flow gas

concentration. Around 15 mg of the synthesized composites was prepared in a stainless-steel sample holder inside a glovebox under an Ar atmosphere. The sample holder was hermetically sealed and transferred to the instrument. Measurements were performed under a 50 mL min^{-1} N_2 (6.0, Linde, Basingstoke, UK) gas flow, and the measurement start temperature of 273 K was achieved with a CryoCooler addon using liquid nitrogen. During the measurement routine, the sample was held at 273 K for 2 h to establish the baseline signal. Then, a temperature ramp of 2 K min^{-1} was applied up to 873 K. Finally, the sample was held at 873 K for 2 h to establish the final baseline signal. All experimental data were treated and plotted using OriginLab 2022 (OriginLab Corporation, Northampton, MA, USA).

3. Results

3.1. Physical Characterisation

The N_2 gas adsorption method was used to determine how ball-milling affected the surface morphology and to determine if $LiAlH_4$ was effectively confined inside the porous structure of the mesoporous carbon black (MCB). All the N_2 gas adsorption measurements were performed at least 30 days after the preparation of the composite to verify the porosity of the composite in equilibrium, and all samples were ball-milled at equivalent conditions before N_2 adsorption measurements for comparability. The N_2 adsorption isotherms (Figure 2a) of the composites exhibit a shape typical of a non-porous material with some mesopores, which is evident from the N_2 uptake at $p/p^\circ > 0.75$. The ball-milled MCB isotherm shape is typical of a micro- and mesoporous material, with some N_2 uptake at low pressures, i.e., $p/p^\circ < 0.01$, in addition to N_2 uptake at $p/p^\circ > 0.75$, which is also confirmed by the considerable specific surface area (S_{BET}) of 230 m^2 g^{-1} and a pore volume (V_{pore}) of 0.34 cm^3 g^{-1} (Figure 2b). The adsorption isotherm and pore size distribution of the ball-milled MCB have been discussed in previous publications in more detail [25,26]. To limit the decomposition of the composite materials, i.e., to not bring forth reactions R1–R3, the degassing was performed at a lower temperature of 313 K in comparison to the 573 K usually used for carbonaceous materials, which possibly left some adsorbed Ar in the materials, and thus, the adsorption isotherms of the $LiAlH_4$/MCB composites were not measured from the lowest p/p° values. This limited the reliable determination of pore size distributions from the measured adsorption isotherms.

The ball-milled $LiAlH_4$ (LAH ball-milled) is practically a non-porous material with an S_{BET} of 8.1 m^2 g^{-1} and a V_{pore} of 0.017 cm^3 g^{-1} (Figure 2b). With the increase in the mass% of $LiAlH_4$ in the composite, the S_{BET} and V_{pore} values decrease (Table 1), but to a higher degree than would be expected from an ideal two-component mixture (Figure 2b). This implies the confinement of $LiAlH_4$ inside the pores of the MCB and the presence of considerable surface interaction between the $LiAlH_4$ and MCB particles inside the composite. The effect was larger at lower $LiAlH_4$ mass%, as very likely the smaller amount of $LiAlH_4$ was confined to a higher degree inside the porous structure of the MCB.

The X-ray diffraction (XRD) (Figure 2c) method was used to qualitatively determine the crystalline phase composition in the $LiAlH_4$/MCB composite materials and the effect of the ball-milling conditions on bulk $LiAlH_4$. Ball-milling of mortared $LiAlH_4$ did not cause noticeable decomposition of the materials, as almost all the diffraction peaks present were from $LiAlH_4$, with the addition of low-intensity Al peaks and the diffuse peak around 2θ of 22° (Figure 2c) caused by the sample holder cap used for hermetically sealing the sample under Ar atmosphere. With the addition of the confining agent, mesoporous carbon black, intense diffraction peaks from Al and Li_3AlH_6 appear. Both Li_3AlH_6 and Al are decomposition products of $LiAlH_4$ from reactions R1 and R2 and R3, respectively. As Li_3AlH_6 crystalline phase is determined, whereas LiH is not, the decomposition during ball-milling is limited by R2. The diffraction peaks from Li_3AlH_6 and Al decreased in intensity with the decrease in the amount of $LiAlH_4$ added to the composite (Figure 2c). This is most likely caused by a combination of the lower presence of $LiAlH_4$ to decompose into large enough Al and Li_3AlH_6 crystallites and by the confinement of the decomposition

products as too small and/or amorphous particles to be detectable by XRD. The effect of higher confinement is especially likely, as even when the diffraction peaks from Al are present, the diffraction peaks from other decomposition products are non-detectable in the case of LAH 20, as they are most likely confined as too small crystallites inside the pores of the MCB (Figure 2c).

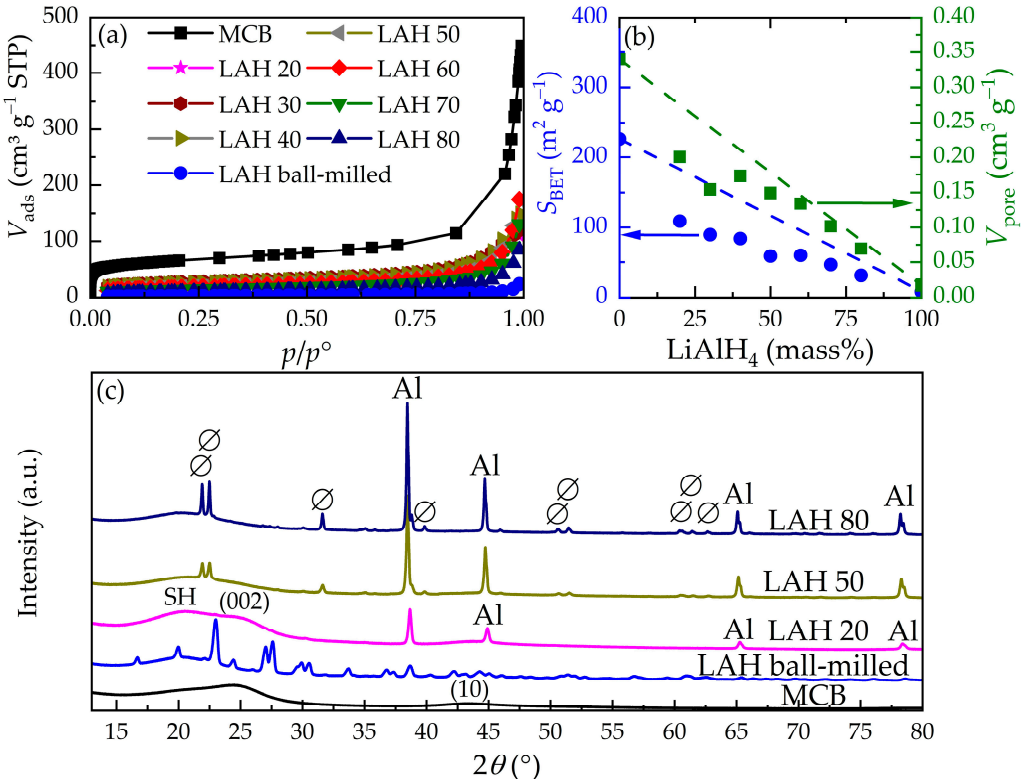

Figure 2. N_2 adsorption isotherms (**a**), specific surface area (S_{BET}) and pore volume (V_{pore}) with idealized linearization of a two-component mixture (dashed line) obtained from N_2 adsorption data (**b**), and X-ray diffractograms (**c**) of bulk ball-milled $LiAlH_4$ (LAH ball-milled), mesoporous carbon black (MCB), and $LiAlH_4$/MCB composites noted as LAH x, where x is the mass% of $LiAlH_4$ in the final composite are noted on top of the corresponding lines. In the X-ray diffractograms (**c**), diffraction peaks from Li_3AlH_4 are noted as Ø, from aluminium as Al, from the sample holder cap as SH, and from the MCB as Miller indices. All the non-labelled diffraction peaks from the LAH ball-milled are from $LiAlH_4$. The diffractograms have been shifted for improved visual presentation.

Table 1. Specific surface area, pore volume, and H_2 release characteristics of the investigated composites.

Compound	S_{BET}/ m^2 g^{-1}	V_{pore}/ cm^3 g^{-1}	$T_{R1,peak}$ [1]/ K	$n_{H2,800K}/n_{H2,theoretical}$ [2]
LAH mortared	-	-	437	0.89
LAH ball-milled	8	0.017	420	0.91
LAH 80	31	0.069	393	0.95
LAH 70	46	0.10	388	0.91
LAH 60	60	0.13	380	0.93
LAH 50	59	0.15	376	0.81
LAH 40	84	0.17	364	0.83
LAH 30	89	0.15	365	0.77
LAH 20	109	0.20	-	0.67
MCB ball-milled	226	0.34		

[1] Temperature of the lowest T H_2 release peak corresponding to H_2 release from the first decomposition reaction, R1. [2] H_2 release efficacy calculated based on the amount of $LiAlH_4$ in the composite calculated from cumulatively released H_2 at 800 K.

3.2. Temperature-Programmed Desorption

Temperature-programmed desorption (TPD) measurements were performed to determine the temperature at which H_2 is released from $LiAlH_4$ and the influence of the confining carbon black (MCB) on the temperature of H_2 release. The TPD measurements were performed within one day after the preparation of the measured composite. Ball-milling of the hand-mortared $LiAlH_4$ decreased the temperature of the main H_2 release peak by 17 K, from 437 K to 420 K (Figure 3a). This is of no great effect by itself, whereas a small amount of H_2 is released at around 380 K from ball-milled $LiAlH_4$, which is most likely caused by the activation of the $LiAlH_4$ surface during ball-milling. With the addition of the MCB, the temperature of the intense H_2 release at around 420 K is decreased to around 380 K in the case of LAH 60 (Table 1), which is more than a 40 K decrease in the temperature of H_2 release. In addition, with the addition of MCB, the onset temperature of H_2 release decreases from 410 K down to the ambient temperature of 295 K, in the case of mortared $LiAlH_4$ and LAH 20, respectively (Figure 3). It must be noted that the influence of MCB on the temperature of H_2 release from the $LiAlH_4$ is not straightforward, as LAH 50 exhibited the lowest onset temperature of hydrogen release from the composite. The release of H_2 was registered almost instantly after the temperature ramp program was started from 273 K. With the increase in the amount of MCB, the peaks of H_2 release (Figure 3a,c) from distinct decomposition reactions become less distinct and more diffuse, as for composites with $LiAlH_4 \leq 60$ mass%, the separation of H_2 from specific decomposition reactions (R1–R3) is not straightforward.

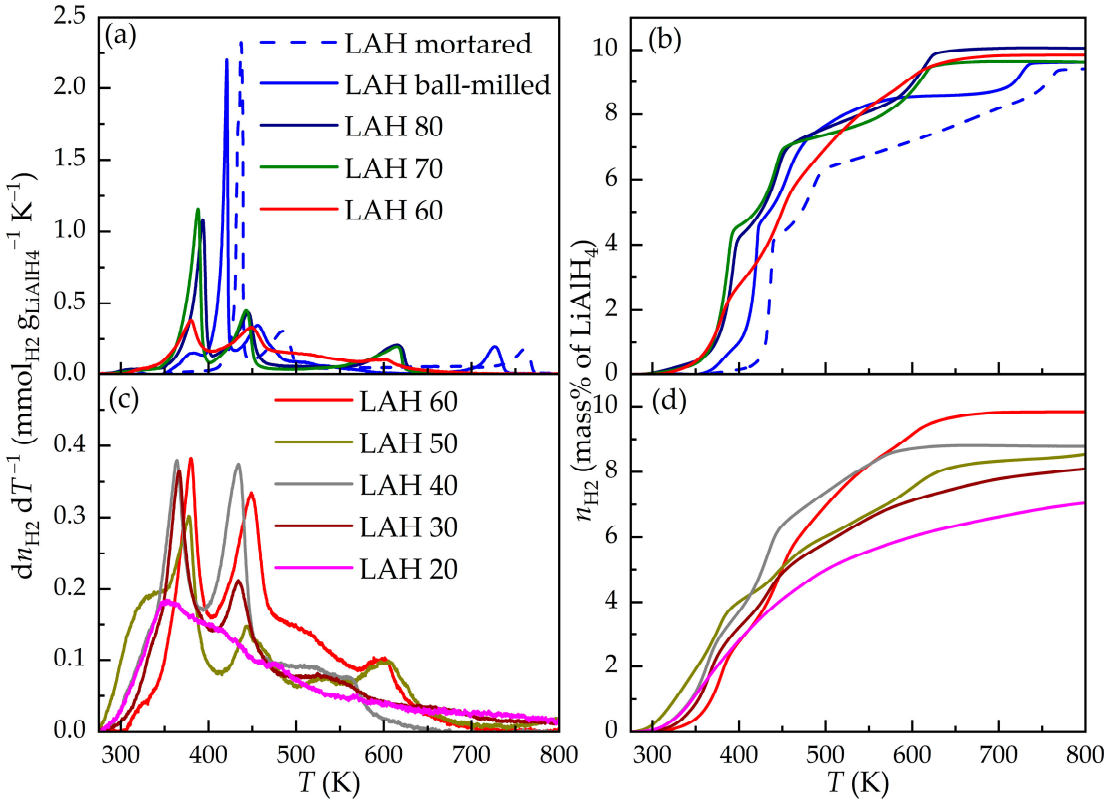

Figure 3. Temperature-programmed desorption (TPD) curves of $LiAlH_4$ (LAH)/mesoporous carbon black (MCB) composites with different LAH content presented as differential (**a**,**c**) and cumulative (**b**,**d**) amounts of released H_2 measured at a temperature ramp rate of 2 K min^{-1}. The TPD curves of LAH/MCB composites have been separated between high LAH content (**a**,**b**) and low LAH content (**c**,**d**).

This is evident from the presentation of H_2 release by cumulative amount (Figure 3b,d), where for $LiAlH_4 < 60$ mass% clear steps, corresponding to well-defined and separated

decomposition steps, are not easily discernible. This is accompanied by a decrease in the total amount of H_2 released upon heating to 800 K, where at 800 K, a total decomposition was measured in the case of both mortared and ball-milled $LiAlH_4$. This is visible from the efficacies of H_2 release, calculated from the theoretical maximum of the H_2 that could be released from the $LiAlH_4$ used in the composite preparation when heated up to 800 K (Table 1). The efficacy decreases with an increase in the amount of MCB added to $LiAlH_4$, from a maximum of 0.95 down to 0.67, in the case of LAH 80 and LAH 20, respectively.

3.3. Decomposition during Storage

The initial release of H_2 at ambient and near-ambient temperatures and the non-linear behaviour of the H_2 release curve vs. mass% of LiAlH4 (Figure 3) signified the possibility of $LiAlH_4$ decomposition at ambient storage conditions, i.e., under 0.1 MPa of Ar and 295 K. To study the stability of the composites during storage, low $LiAlH_4$ mass% composites, namely LAH 20, LAH 30, and LAH 40, were characterized with temperature-programmed desorption, X-ray diffraction, and N_2 adsorption measurements after a certain time had passed from the ball-milling synthesis (Figure 4).

Over time in storage under 0.1 MPa of Ar, the H_2 release at lower temperatures (<420 K) decreases (Figure 4a–d) considerably. This is most notably evident from the disappearance of the well-defined peak corresponding to the first decomposition reaction, R1, at 370 K. This is especially well pronounced for the higher $LiAlH_4$ mass% composites under study, LAH 30 (Figure 4c) and LAH 40 (Figure 4d). The decrease in the amount of H_2 released at low temperatures coincides with a lower total amount of H_2 released (Figure 4b) and with a very low final efficacy (Table 2), i.e., the amount of H_2 released at 800 K in comparison to the maximum theoretical amount of H_2 in the composite based on the amount of $LiAlH_4$ in the composite. In the case of LAH 30, the TPD curves are practically identical after 14 and after 23 days of storage (Figure 4c), which implies that for LAH 30, the decomposition of the composite was reached during the first 14 days. For all the measured composites, there was an initial shift of H_2 release towards higher temperatures, to the second peak of H_2 release at around 430 K, during the initial 7 days under storage (Figure 4a,c,d). When stored beyond 7 days, a slight shift of H_2 release towards lower temperatures with a considerable decrease in the amount of H_2 released from the second peak at around 430 K, was evident in the case of LAH 20 and LAH 30 (Figure 4a,c). The decrease in the amount of H_2 released is accompanied by the increase in the specific surface area and pore volume (Table 2), where both increase almost two-fold after storage under 0.1 MPa of Ar over 30 days. X-ray diffraction measurements with equivalent time steps were performed for LAH 20 (Figure 4e). Al was present after the synthesis, and diffraction peaks corresponding to Al increased in intensity during 7 days of storage. In addition, low-intensity diffraction peaks corresponding to Li_3AlH_6 were only detected after 7 days of storage, which implicates the formation of an intermediate crystalline Li_3AlH_6 phase.

Table 2. Characteristic properties of porosity and H_2 release of LAH 20 after different storage times.

t/days	S_{BET}/ $m^2\ g^{-1}$	V_{pore}/ $cm^3\ g^{-1}$	$n_{H2,800K}/n_{H2,theoretical}$ [1]
1	52	0.12	0.69
7	89	0.16[1]	0.34
30	109	0.20	0.16

[1] H_2 release efficacy calculated based on the amount of $LiAlH_4$ in the composite calculated from cumulatively released H_2 at 800 K.

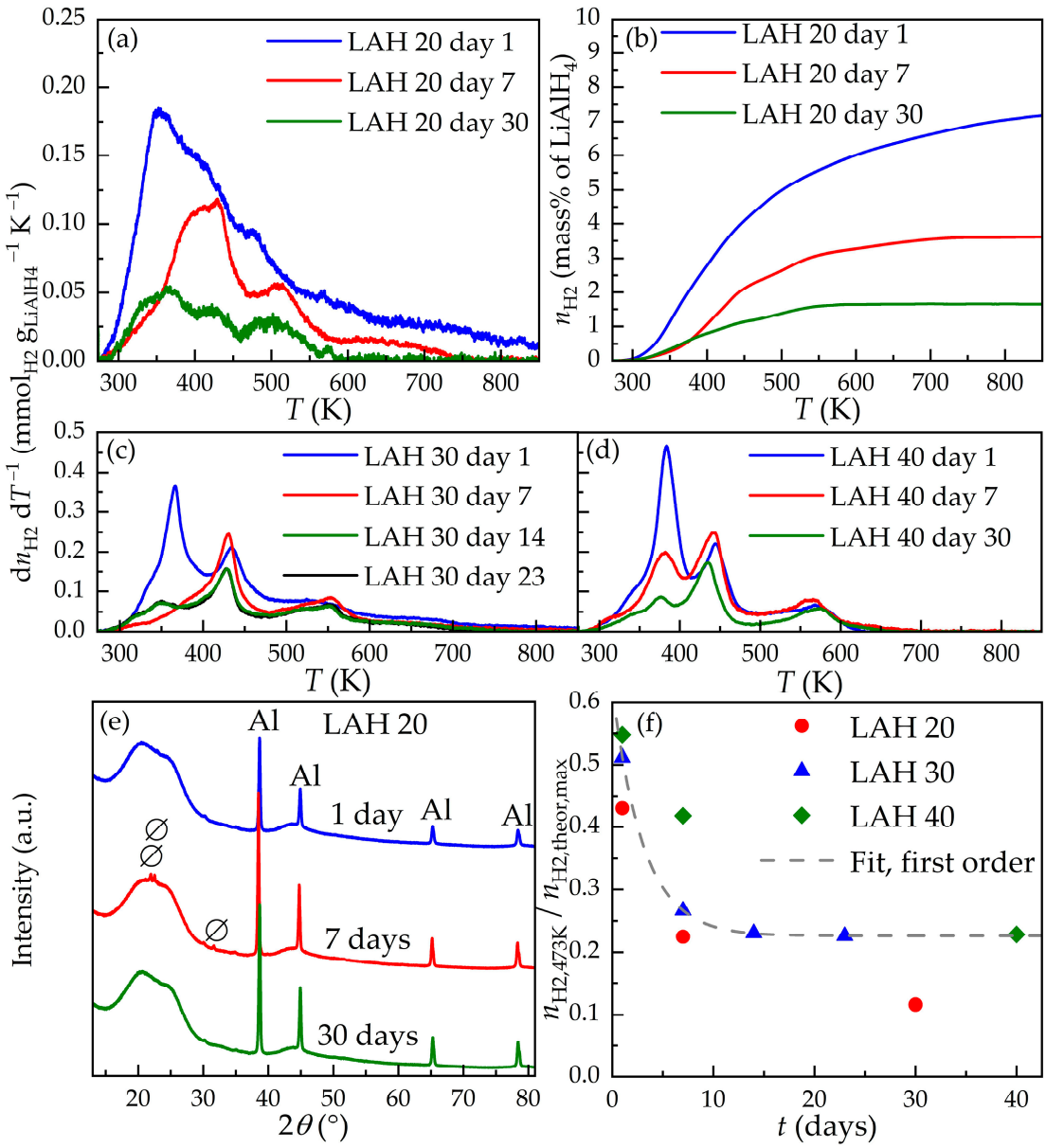

Figure 4. Temperature-programmed desorption curves measured at a temperature ramp rate of 2 K min^{-1} for LAH 20 (**a**,**b**), LAH 30 (**c**), and LAH 40 (**d**) presented as differential (**a**,**c**,**d**) and cumulative (**b**) amounts of H_2 released and X-ray diffractograms (**e**) of LAH 20 after different storage times under an inert gas atmosphere. Here, the X-ray diffractogram (**e**) Ø notes diffraction peaks from Li_3AlH_6 and Al notes diffraction peaks from aluminium, and the diffractograms have been shifted for improved visual presentation. The efficacy of H_2 released in comparison to maximum theoretical H_2 content (**f**) upon heating to 473 K vs. storage time with the fit (grey dashed line) to the first-order reaction kinetics for LAH 30.

The efficacy of the released H_2 when heated up to 473 K decreases with time in storage under 0.1 MPa of Ar (Figure 4f), where the efficacy when heated to 473 K is of interest, as the change in the amount of H_2 released at such low temperatures is primarily influenced by the first two decomposition reactions, R1 and R2. This is also mirrored by the decrease in efficacy when heated to 800 K (Table 2). LAH 30 included four TPD measurements over different storage times vs. three for LAH 20 and LAH 40, and the equilibrium was reached after 14 days and 23 days of storage (Figure 4c,f), based on the TPD measurements. Thus,

the efficacy vs. storage time data of LAH 40 was fitted with an equation corresponding to a first-order chemical reaction:

$$n_{\mathrm{H2,473K}}/n_{\mathrm{H2,theor,max}} = n_0\, e^{(-k\,t)} + n_{\mathrm{final}}, \quad (1)$$

where n_0 is the initial efficacy of the component that releases H_2 over time in storage, k is the rate constant in units of day^{-1}, t is storage time in days, and n_{final} is the efficacy of the composite retained after all the decomposition during storage has finished and the composite is at an equilibrium state.

The fit of the efficacy vs. storage time of LAH 30 (Figure 4f) to Equation (1) obtained a k value of 0.33 day^{-1}, which is most likely, based on visual comparison (Figure 4f), higher than that for LAH 20 and LAH 40. The obtained n_0 value is 0.40, which means that 40% of the theoretical maximum amount of H_2 is released during storage under 0.1 MPa of Ar. LAH 20 and LAH 40 exhibit similar trends in the difference of efficacy, being around 0.3 between the 1st day and 30th day of storage, similar to that for LAH 30 (0.29). The n_{final} value for LAH 30 is 0.23; thus, upon heating to 473 K, the amount of stored H_2 in a stable form is 23% of the theoretical maximum amount of H_2 contained in the $LiAlH_4$ used for the LAH 30 composite, regardless of time in storage. A similar trend was exhibited for LAH 40 (Figure 4f), whereas almost all H_2 storage capability was lost in LAH 20 upon storage under 0.1 MPa of Ar. Only around 10% of the theoretically contained H_2 is released upon heating to 473 K after 30 days of storage.

4. Discussion

The use of mesoporous carbon black (MCB) as a confining agent even at low amounts, 20 mass%, with a ball-milling-based composite preparation process is shown to decrease the onset temperature of H_2 release by 30 K in comparison to ball-milling bulk $LiAlH_4$ without any additive. The main peak of H_2 release, from the first reaction R1, is around the working temperature of high-temperature polymer electrolyte fuel cells [31], namely 390 K, which would allow the use of waste heat from fuel cells for the release of H_2. With the use of a lower $LiAlH_4$ to MCB content, $\leq$60 mass% of $LiAlH_4$ in the final composite, the release of H_2 from the R1 reaction, characteristically present as a sharp peak in the TPD curves, became more diffuse and disappeared at the lowest investigated $LiAlH_4$ to an MCB content of 20 mass%. In addition, for all composite material syntheses, the presence of Al was detected by XRD (Figure 2c), and a clear decrease in the efficacy (Table 1) of the released H_2 in comparison to the theoretical maximum was determined when the $LiAlH_4$ content to MCB was decreased to $\leq$50 mass%.

In addition to the decomposition of the $LiAlH_4$ inside the composite during the ball-milling preparation process, a considerable amount of up to 40% (Figure 4f and fitting to Equation (1)) of the theoretical maximum H_2 content was released during storage over multiple days at ambient temperature, 295 K, and under 0.1 MPa of Ar. The 40% amount of H_2 released over time in storage corresponds to the almost complete decomposition of $LiAlH_4$ to Li_3AlH_4 (R1), where R1 would release 50% of the H_2 contained in $LiAlH_4$. By contrast, the high equilibrium pressure, $\geq$100 MPa, of $LiAlH_4$ has been shown beforehand [9,21], based on which $LiAlH_4$ should decompose to release H_2 at ambient temperature conditions, practical applicability has not been reached because of the kinetic barrier towards going from the initial pseudo-equilibrium of $LiAlH_4$ towards to real equilibrium state of Li_3AlH_6. This work exemplifies the possibility of considerably destabilizing $LiAlH_4$ using confinement inside a mesoporous carbon black, in addition to previously showcased catalysts, for low-temperature H_2 release. We also demonstrate the importance of confined complex metal hydride composite storage conditions, where the H_2 storage materials should be stored under H_2 pressure and tested under different pressure conditions to be certain to probe the properties of pristine composites and compounds and, thus, lessen the variability between different experimental works.

The release of H_2 at ambient temperature conditions over several days also affords to indulge in the possibility of hydrogenating such materials under relatively mild tempera-

ture and H_2 pressure conditions, which is a vital aspect for practical applicability. Thus, we present the confinement of $LiAlH_4$ in a mesoporous carbon black for the destabilization of $LiAlH_4$ and bring forth the first decomposition reaction, releasing 50% of the stored H_2, at ambient conditions with the potential for hydrogenation at relatively mild temperature and H_2 pressure conditions.

Author Contributions: Conceptualization, P.R., K.T. and R.P.; methodology, P.R. and R.P.; formal analysis, P.R., R.P. and J.A.; investigation, P.R., K.T. and R.P.; resources, M.M. and E.L.; data curation, P.R.; writing—original draft preparation, R.P. and P.R.; writing—review and editing, P.R., K.T., M.M., E.L. and J.A.; visualization, P.R. and R.P.; supervision, R.P., M.M. and E.L.; project administration, E.L. and R.P.; funding acquisition, M.M. and E.L. All authors have read and agreed to the published version of the manuscript.

Funding: This research was supported by the EU through the European Regional Development Fund (Centers of Excellence, TK141 "Advanced materials and high-technology devices for energy recuperation systems"), by the Estonian Research Council Grants, grant numbers PUTJD957 and PRG676, and by the Swedish Research Council through a neutron project grant (Dnr. 2016-06955 and Dnr. 2021-06157). R.P. was funded by a postdoctoral scholarship awarded by Dr. Ragnar Holm's Foundation at KTH, Sweden.

Data Availability Statement: The data presented in this study are available on request from the corresponding author.

Acknowledgments: The authors would also like to extend their gratitude towards Jaan Aruväli and Kalle Kirsimäe from the Institute of Ecology and Earth Sciences at the University of Tartu for providing access and performing the XRD measurements.

Conflicts of Interest: The authors declare no conflict of interest. The funders had no role in the design of the study; in the collection, analyses, or interpretation of data; in the writing of the manuscript; or in the decision to publish the results.

References

1. Ku, A.Y.; Kocs, E.A.; Afzal, S.; Ewan, M.; Glenn, J.R.; Toma, F.; Vickers, J.; Weeks, B.; White, A.A. Opportunities for the Materials Research Community to Support the Development of the H_2 Economy. *MRS Energy Sustain.* **2023**. [CrossRef]
2. Nazir, H.; Muthuswamy, N.; Louis, C.; Jose, S.; Prakash, J.; Buan, M.E.M.; Flox, C.; Chavan, S.; Shi, X.; Kauranen, P.; et al. Is the H_2 Economy Realizable in the Foreseeable Future? Part III: H_2 Usage Technologies, Applications, and Challenges and Opportunities. *Int. J. Hydrogen Energy* **2020**, *45*, 28217–28239. [CrossRef] [PubMed]
3. Nazir, G.; Rehman, A.; Hussain, S.; Aftab, S.; Heo, K.; Ikram, M.; Patil, S.A.; Aizaz Ud Din, M. Recent Advances and Reliable Assessment of Solid-State Materials for Hydrogen Storage: A Step Forward toward a Sustainable H_2 Economy. *Adv. Sustain. Syst.* **2022**, *6*, 2200276. [CrossRef]
4. Nazir, H.; Muthuswamy, N.; Louis, C.; Jose, S.; Prakash, J.; Buan, M.E.; Flox, C.; Chavan, S.; Shi, X.; Kauranen, P.; et al. Is the H_2 Economy Realizable in the Foreseeable Future? Part II: H_2 Storage, Transportation, and Distribution. *Int. J. Hydrogen Energy* **2020**, *45*, 20693–20708. [CrossRef]
5. So, S.H.; Sung, S.J.; Yang, S.J.; Park, C.R. Where to Go for the Development of High-Performance H_2 Storage Materials at Ambient Conditions? *Electron. Mater. Lett.* **2023**, *19*, 1–18. [CrossRef]
6. Løvvik, O.M.; Opalka, S.M.; Brinks, H.W.; Hauback, B.C. Crystal Structure and Thermodynamic Stability of the Lithium Alanates $LiAlH_4$ and Li_3AlH_6. *Phys. Rev. B* **2004**, *69*, 134117. [CrossRef]
7. Dymova, T.N.; Aleksandrov, D.P.; Konoplev, V.N.; Silina, T.A.; Sizareva, A.S. Spontaneous and Thermal-Decomposition of Lithium Tetrahydroaluminate $LiAlH_4$-the Promoting Effect of Mechanochemical Action on the Process. *Koord. Khimiya* **1994**, *20*, 279–285.
8. Ares, J.R.; Aguey-Zinsou, K.-F.; Porcu, M.; Sykes, J.M.; Dornheim, M.; Klassen, T.; Bormann, R. Thermal and Mechanically Activated Decomposition of $LiAlH_4$. *Mater. Res. Bull.* **2008**, *43*, 1263–1275. [CrossRef]
9. Jang, J.-W.; Shim, J.-H.; Cho, Y.W.; Lee, B.-J. Thermodynamic Calculation of $LiH \leftrightarrow Li_3AlH_6 \leftrightarrow LiAlH4$ Reactions. *J. Alloys Compd.* **2006**, *420*, 286–290. [CrossRef]
10. Sazelee, N.A.; Ismail, M. Recent Advances in Catalyst-Enhanced $LiAlH_4$ for Solid-State Hydrogen Storage: A Review. *Int. J. Hydrogen Energy* **2021**, *46*, 9123–9141. [CrossRef]
11. Varin, R.A.; Zbroniec, L. Decomposition Behavior of Unmilled and Ball Milled Lithium Alanate ($LiAlH_4$) Including Long-Term Storage and Moisture Effects. *J. Alloys Compd.* **2010**, *504*, 89–101. [CrossRef]
12. Cho, Y.; Li, S.; Snider, J.L.; Marple, M.A.T.; Strange, N.A.; Sugar, J.D.; El Gabaly, F.; Schneemann, A.; Kang, S.; Kang, M.; et al. Reversing the Irreversible: Thermodynamic Stabilization of $LiAlH_4$ Nanoconfined Within a Nitrogen-Doped Carbon Host. *ACS Nano* **2021**, *15*, 10163–10174. [CrossRef] [PubMed]

13. Che Mazlan, N.S.; Asyraf Abdul Halim Yap, M.F.; Ismail, M.; Yahya, M.S.; Ali, N.A.; Sazelee, N.; Seok, Y.B. Reinforce the Dehydrogenation Process of $LiAlH_4$ by Accumulating Porous Activated Carbon. *Int. J. Hydrogen Energy* **2023**, *48*, 16381–16391. [CrossRef]
14. Pratthana, C.; Yang, Y.; Rawal, A.; Aguey-Zinsou, K.-F. Nanoconfinement of Lithium Alanate for Hydrogen Storage. *J. Alloys Compd.* **2022**, *926*, 166834. [CrossRef]
15. Wang, L.; Rawal, A.; Quadir, M.Z.; Aguey-Zinsou, K.-F. Nanoconfined Lithium Aluminium Hydride ($LiAlH_4$) and Hydrogen Reversibility. *Int. J. Hydrogen Energy* **2017**, *42*, 14144–14153. [CrossRef]
16. Zhang, C.; Liang, L.; Zhao, S.; Wu, Z.; Wang, S.; Yin, D.; Wang, Q.; Wang, L.; Wang, C.; Cheng, Y. Dehydrogenation Behavior and Mechanism of $LiAlH_4$ Adding Nano-CeO_2 with Different Morphologies. *Nano Res.* **2023**, *16*, 9426–9434. [CrossRef]
17. Liu, S.-S.; Li, Z.-B.; Jiao, C.-L.; Si, X.-L.; Yang, L.-N.; Zhang, J.; Zhou, H.-Y.; Huang, F.-L.; Gabelica, Z.; Schick, C.; et al. Improved Reversible Hydrogen Storage of $LiAlH_4$ by Nano-Sized TiH_2. *Int. J. Hydrogen Energy* **2013**, *38*, 2770–2777. [CrossRef]
18. Rafi-ud-din; Zhang, L.; Ping, L.; Xuanhui, Q. Catalytic Effects of Nano-Sized TiC Additions on the Hydrogen Storage Properties of $LiAlH_4$. *J. Alloys Compd.* **2010**, *508*, 119–128. [CrossRef]
19. Cheng, H.; Zheng, J.; Xiao, X.; Liu, Z.; Ren, X.; Wang, X.; Li, S.; Chen, L. Ultra-Fast Dehydrogenation Behavior at Low Temperature of $LiAlH_4$ Modified by Fluorographite. *Int. J. Hydrogen Energy* **2020**, *45*, 28123–28133. [CrossRef]
20. Chen, J.; Kuriyama, N.; Xu, Q.; Takeshita, H.T.; Sakai, T. Reversible Hydrogen Storage via Titanium-Catalyzed $LiAlH_4$ and Li_3AlH_6. *J. Phys. Chem. B* **2001**, *105*, 11214–11220. [CrossRef]
21. Brinks, H.W.; Fossdal, A.; Fonneløp, J.E.; Hauback, B.C. Crystal Structure and Stability of $LiAlD_4$ with TiF^3 Additive. *J. Alloys Compd.* **2005**, *397*, 291–295. [CrossRef]
22. Gao, J.; Adelhelm, P.; Verkuijlen, M.H.W.; Rongeat, C.; Herrich, M.; van Bentum, P.J.M.; Gutfleisch, O.; Kentgens, A.P.M.; de Jong, K.P.; de Jongh, P.E. Confinement of $NaAlH_4$ in Nanoporous Carbon: Impact on H_2 Release, Reversibility, and Thermodynamics. *J. Phys. Chem. C* **2010**, *114*, 4675–4682. [CrossRef]
23. Palm, R.; Kurig, H.; Aruväli, J.; Lust, E. $NaAlH_4$/Microporous Carbon Composite Materials for Reversible Hydrogen Storage. *Microporous Mesoporous Mater.* **2018**, *264*, 8–12. [CrossRef]
24. Tuul, K.; Palm, R. Influence of Nanoconfinement on the Hydrogen Release Processes from Sodium Alanate. *Reactions* **2021**, *2*, 1. [CrossRef]
25. Tuul, K.; Palm, R.; Aruväli, J.; Lust, E. Dehydrogenation and Low-Pressure Hydrogenation Properties of $NaAlH_4$ Confined in Mesoporous Carbon Black for Hydrogen Storage. *Int. J. Hydrogen Energy* **2023**, *48*, 19646–19656. [CrossRef]
26. Palm, R.; Tuul, K.; Elson, F.; Nocerino, E.; Forslund, O.K.; Hansen, T.C.; Aruväli, J.; Månsson, M. In Situ Neutron Diffraction of $NaAlD_4$/Carbon Black Composites during Decomposition/Deuteration Cycles and the Effect of Carbon on Phase Segregation. *Int. J. Hydrogen Energy* **2022**, *47*, 34195–34204. [CrossRef]
27. Santiago, D.; Rodríguez-Calero, G.G.; Rivera, H.; Tryk, D.A.; Scibioh, M.A.; Cabrera, C.R. Platinum Electrodeposition at High Surface Area Carbon Vulcan-XC-72R Material Using a Rotating Disk-Slurry Electrode Technique. *J. Electrochem. Soc.* **2010**, *157*, F189. [CrossRef]
28. Lázaro, M.J.; Calvillo, L.; Celorrio, V.; Pardo, J.; Perathoner, S.; Moliner, R. Study and Application of Vulcan XC-72 in Low Temperature Fuel Cells. In *Carbon Black: Production, Properties and Uses*; Nova Science Publishers, Inc.: Hauppauge, NY, USA, 2011; pp. 41–68, ISBN 978-1-61209-535-6.
29. Thommes, M.; Kaneko, K.; Neimark, A.V.; Olivier, J.P.; Rodriguez-Reinoso, F.; Rouquerol, J.; Sing, K.S.W. Physisorption of Gases, with Special Reference to the Evaluation of Surface Area and Pore Size Distribution (IUPAC Technical Report). *Pure Appl. Chem.* **2015**, *87*, 1051–1069. [CrossRef]
30. Kabekkodu, S.N.; Faber, J.; Fawcett, T. New Powder Diffraction File (PDF-4) in Relational Database Format: Advantages and Data-Mining Capabilities. *Acta Crystallogr. B* **2002**, *58*, 333–337. [CrossRef]
31. Zhang, J.; Xie, Z.; Zhang, J.; Tang, Y.; Song, C.; Navessin, T.; Shi, Z.; Song, D.; Wang, H.; Wilkinson, D.P.; et al. High Temperature PEM Fuel Cells. *J. Power Sources* **2006**, *160*, 872–891. [CrossRef]